metals

MDPI

Article

Investigation of the Structural State of a Liquid Mg–Zn Magnesium Alloy from the Perspective of the Behavior of the Bjerrum–Guggenheim Osmotic Coefficient in the Melt

Vera Tolokonnikova [1], Sailaubai Baisanov [1], Amankeldy Ahmetov [1], Yerbolat Makhambetov [1], Olzhas Kenzhaliyev [2] and Alexey Orlov [1,*]

[1] Chemical-Metallurgical Institute Named After Zh. Abishev, 100009 Karaganda, Kazakhstan; tolokon-splav@bk.ru (V.T.); splav_sailaubai2021@mail.ru (S.B.); aman1aotero@qmail.com (A.A.); makhambetovyerbolat@gmail.com (Y.M.)

[2] Department of Artificial Intelligence Technologies, Karaganda Industrial University, 101400 Temirtay, Kazakhstan; andas89@gmail.com

* Correspondence: wolftailer@mail.ru

Abstract

Carrying out a series of fundamental studies in the field of physicochemical analysis, based on an approach that considers the phase state of alloys and accounts for the regular patterns of interaction of substances in multicomponent ores that are complex in both chemical and phase composition, makes it possible to formulate a number of scientifically substantiated practical recommendations. The aim of this work is to assess the degree of zinc sublimation from a magnesium alloy through the behavior of the Bjerrum–Guggenheim osmotic coefficient and the degree of dissociation of the congruent compound. The paper presents a method for processing phase equilibrium lines in a temperature–composition phase diagram, resulting in mathematical expressions for the liquidus and solidus lines on a unified analytical basis in the form of a semi-empirical dependence derived from the Schröder–Le Chatelier equation. Indirectly, through the Bjerrum–Guggenheim osmotic coefficient, the degree of dissociation of $MgZn_2$ in the Mg–Zn system was determined to range from 17% to 46%. This result is in good agreement with the conclusions of Nikolay Semyonovich Kurnakov regarding the degree of dissociation of congruent compounds inferred from the shape of the maximum on phase diagrams. For $MgZn_2$, this maximum is very smooth, i.e., the composition of the liquid phase changes continuously with deviation from stoichiometry, resulting in a symmetrical rounded peak. An experimental study was carried out using a SEM/EDS analytical complex to confirm the high volatility of zinc. The key zinc-concentrating phases were identified in the investigated processing products (slag, metal, and dust), which is consistent with the theoretical premises and explains the mechanism of zinc behavior during high-temperature processing of zinc-containing slags. The form of zinc occurrence in different phases was established. In the initial slag, the zinc content reaches 51.79%. In the metallic phase, zinc is detected as fine dispersed inclusions. In the collected dust (flue ducts), particles enriched in zinc up to 44.09 wt.% were identified.

Keywords: phase diagrams; liquidus and solidus lines; bjerrum–guggenheim osmotic coefficient; mathematical model; activity; degree of dissociation; volatility

Check for updates

Academic Editor: Manoj Gupta

Received: 22 June 2026
Revised: 5 August 2026
Accepted: 15 August 2026
Published: 20 August 2026

Copyright: © 2026 by the authors. Licensee MDPI, Basel, Switzerland. This article is an open access article distributed under the terms and conditions of the Creative Commons Attribution (CC BY) license.

1. Introduction

The development of new alloys and the design of manufacturing technologies based on them at the current stage of scientific advancement require the establishment of a new

direction in materials science, namely, computational thermodynamics, which integrates thermodynamic and physical chemistry calculation methods with computer-based simulation tools. The very concept of "modeling" inherently implies the use of a mathematical model. Historically, thermodynamic models have undergone significant evolution, progressing from ideal solutions to regular solutions, subregular solution models, associated liquid models, pseudopotential models, and others.

In recent decades, owing to advances in software development and numerical methods, the CALPHAD (CALculation of PHAse Diagrams) approach has emerged alongside classical methods of physicochemical analysis. This method integrates all available thermodynamic and experimental information on phase equilibria obtained from thermophysical and thermochemical studies. The properties of each phase are then described using an appropriate mathematical model.

Widely used and accessible thermodynamic databases and software packages for studying the scientific principles of thermodynamic modeling of phase equilibria include Thermo-Calc, FactSage, Pandat, POLYTHERM, and others.

Significant progress has recently been achieved in the development of thermodynamic theories describing metallic melts. In particular, alongside the theories of regular and subregular solutions, more advanced models have been developed, including the modified quasichemical model, the surrounded atom theory, and the cluster theory of solutions. All these approaches are based on the assumption that the properties and structure of metallic melts are primarily determined by the size of constituent particles and the forces of interparticle interactions.

Despite their advantages, all of the aforementioned approaches share a common limitation: they require the preliminary determination of interaction parameters and, in many cases, the enthalpy of mixing of liquid alloys, which necessitates additional experimental investigations. Furthermore, the mathematical framework of each model and its modifications is often applicable only to specific groups of systems. For other systems, the development of specialized mathematical formulations or the introduction of complex correction factors becomes necessary.

The relevance of the present study lies in the development of a unified physicochemical model describing the structure of liquid metallurgical melts, capable of predicting equilibrium relationships between individual phases over a wide range of compositions and temperatures. The absence of an adequate physical model of the liquid state in metallurgical systems remains a major obstacle to establishing functional relationships between variations in thermodynamic and physicochemical properties in multicomponent heterogeneous systems.

Solving the problem of the dissociation of congruently melting compounds during high-temperature processes is of considerable practical importance for the development of technologies for producing semiconductor compounds with a predetermined degree of structural defects. It is also essential for designing complex semiconductor alloying processes involving donor–acceptor interactions, which are fundamentally equivalent to the dissociation reactions of the corresponding compounds.

The processing of polymetallic ores and technogenic products of their metallurgical treatment is among the most challenging tasks of modern pyrometallurgy. The complex chemical and phase composition of such raw materials, the presence of stable intermetallic and oxide compounds, as well as the mutual influence of components in the melt, significantly hinder the selective extraction of target metals. To date, no universal technological solution has been developed that ensures the comprehensive recovery of valuable components with minimal losses and energy consumption [1].

The structural state of the melt and the nature of interparticle interactions between components play a crucial role in high-temperature processing. The behavior of elements in the melt is governed by their thermodynamic activity, their tendency to form congruent and incongruent compounds, and the degree of their dissociation. These factors directly affect phase equilibria, the volatility of individual components, and the distribution of elements among the metallic, slag, and gas phases.

Zinc, as one of the characteristic components of polymetallic raw materials and slags, exhibits high volatility at elevated temperatures, which necessitates a thorough thermodynamic analysis of its behavior in multicomponent systems. A promising approach to describing such systems is the application of physicochemical analysis methods based on the treatment of phase diagrams and the determination of thermodynamic characteristics using semi-empirical relationships, in particular the Schroeder–Le Chatelier equation.

The analysis of liquidus and solidus lines, as well as the evaluation of the Bjerrum–Guggenheim osmotic coefficient, makes it possible to indirectly determine the degree of dissociation of congruent compounds and to reveal patterns in the variation in component activity in the melt. This approach provides a theoretical basis for explaining the mechanisms of zinc volatilization and its redistribution between phases during the processing of zinc-containing slags.

Thus, the integrated combination of thermodynamic modeling and experimental investigations of the phase composition of smelting products makes it possible to substantiate the mechanism of zinc behavior under high-temperature processing of multicomponent systems and to formulate practical recommendations for improving the efficiency of valuable component recovery [2,3].

2. Materials and Methods

This paper is a continuation of study [4], which presented a methodology for the mathematical description of phase equilibrium lines based on the analysis of phase crystallization fields in various systems.

For a clearer understanding of the approach adopted in the present work, we provide the principal equations used to analyze the behavior of components in the melt of the binary Mg–Zn system [5].

For ideal systems forming solid and liquid solutions, the equilibrium phase compositions vary along the liquidus and solidus lines in accordance with the Schröder–Le Chatelier equation [5,6]:

$$\ln \frac{a^{L}_{1,id}}{a^{S}_{1,id}} = \frac{\Delta H_{m,i,1}}{R}\left(\frac{1}{T_{m,i,1}} - \frac{1}{T}\right) + \int_{T}^{T_{m,i,1}}\left[\frac{1}{RT^2}\int_{T}^{T_{m,i,1}} \Delta C_{p,1} dT\right] dT, \quad (1)$$

where $\Delta H_{m,1(2)}$—is the enthalpy of fusion of components 1 and 2 at their melting temperatures, J/mol;

R is the universal gas constant, J/(mol·K).

$T_{m,i}$ and T are the melting temperature of component 1 and the crystallization temperature of the melt, K.

As a measure of deviation from ideality, the well-known Bjerrum–Guggenheim osmotic coefficient (Φ_i) was used [6]. For solid–liquid equilibrium, it is expressed as:

$$Ln\ a_i = \Phi_i * Ln\ X_i \quad (2)$$

In physicochemical literature, this coefficient is referred to as the osmotic coefficient [6]. It establishes a relationship between the activity and concentration of a component in

solution, which differs significantly from the analogous relationship between the activity coefficient and concentration. In this formulation, the coefficient, unlike the activity coefficient γ_i, characterizes the degree of deviation of the partial Gibbs free energy (chemical potential) of component (i) in the solution (melt) from its ideal contribution, i.e., $\mu_i = RT \ln a_i = RT \ln X_i[\mu_{i,id}] + RT \ln \gamma_i$ where X_i is the mole fraction and γ_i is the activity coefficient, with $a_i = x_i \cdot \gamma_i$. Hence,

$$\Phi_i = \frac{\mu_i}{\mu_{i,id}} = \frac{RT \ln a_i}{RT \ln X_i} = \ln a_i / \ln X_i \quad (3)$$

This coefficient is generally used to describe the partial thermodynamic properties of components and represents their energetic characteristic, whereas the activity coefficient γ_i serves as a concentration-dependent parameter. In practice, the coefficient Φ is used relatively infrequently because its introduction considerably complicates the differential equations of solution thermodynamics. It is most commonly employed in studies of osmotic phenomena in electrolyte solutions.

For the solid–liquid equilibrium, where the reaction $S \rightarrow L$ takes place, i.e., a chemical process is involved, the coefficient Φ can be expressed in the following form:

$$\Phi_i = \frac{\Delta G^{S \rightarrow L}_{m,i}}{\Delta G^{S \rightarrow L}_{m,i,id}} = \frac{\mu^L_i - \mu^S_i}{\mu^L_{i,id} - \mu^S_{i,id}} = \frac{RT \ln(a^L_i / a^S_i)}{RT \ln(x^L_i / x^S_i)} = 1 + \frac{\ln \gamma^L_i / \ln \gamma^S_i}{\ln x^L_i / \ln x^S_i}. \quad (4)$$

Accordingly, in the generalized form, the variation in the partition coefficients of the components between the solid and liquid phases along the liquidus and solidus lines of phase diagrams can be expressed as follows:

$$\ln \frac{X^L_1}{X^S_1} = \frac{\ln(a^L_1 / a^S_1)}{\Phi_1} \text{ и } \quad \ln \frac{X^L_2}{X^S_2} = \frac{\ln(a^L_2 / a^S_2)}{\Phi_2} \quad (5)$$

where $\Phi_{1,2}$ are the Bjerrum–Guggenheim coefficients of components 1 and 2, respectively.

Accordingly, the ratio of the activities of the components in the melt and in the solid solution along the phase equilibrium line at a given temperature for real systems is determined using the Schröder–Le Chatelier Equation (1). For components 1 and 2, Equations (6) and (7) take the following form:

$$\ln \frac{a^L_1}{a^S_1} = \ln \frac{X^L_{1,id}}{X^S_{1,id}} = \frac{\Delta H_{m,i,1}}{R} \left(\frac{1}{T_{m,i,1}} - \frac{1}{T} \right) + \int_T^{T_{m,i,1}} \left[\frac{1}{RT^2} \int_T^{T_{m,i,1}} \Delta c_{p,1} dT \right] dT, \quad (6)$$

$$\ln \frac{a^L_2}{a^S_2} = ln \frac{X^L_{2,id}}{X^S_{2,id}} = \frac{\Delta H_{m,i,2}}{R} \left(\frac{1}{T_{m,i,2}} - \frac{1}{T} \right) + \int_T^{Tm,i,2} \left[\frac{1}{RT^2} \int_T^{T_{m,i,2}} \Delta c_{p,2} dT \right] dT. \quad (7)$$

where $\Delta H_{m,1(2)}$ is the enthalpy of fusion of components 1 and 2 at their respective melting temperatures, J/(mol·K); R is the universal gas constant, J/(mol·K); $T_{m,1(2)}$ and T are the melting temperatures of components 1 and 2 and the crystallization temperature of the melt, respectively, K; and $\Delta C_{p,1(2)}$ is the change in heat capacity upon melting of the corresponding components.

Since the Bjerrum–Guggenheim osmotic coefficient (Φ) characterizes the degree of deviation of the energetic state of a given component from ideality under equilibrium conditions, this deviation increases with the strength of the interaction between that component and the other constituents of the system. Such interactions can be divided into two contributions: van der Waals interactions (interatomic or intermolecular interactions

that are inevitably present in the melt of any system) and directional interactions (associated with the formation of directional heteropolar and homopolar bonds between components in the melt, i.e., the formation of clusters).

In both cases, the interaction strength between the component under consideration and the second component, both in the melt and in the solid solution, and consequently the degree to which its properties deviate from ideal behavior, depends on the amounts of this component present in each of the two phases.

According to the statistical thermodynamics' theory, the former is defined as $\exp\left(-\frac{\Delta G^0_{m,i}}{RT}\right)$, whereas the latter is expressed as the difference between the number of particles in the fully associated state and those in the free state. Therefore, the variation in the osmotic coefficient Φ_i along the phase equilibrium line can be represented in the following form:

$$\Phi_i = A_i + B_i \cdot \exp\left(-\frac{\Delta G^0_{m,i}}{RT}\right) \tag{8}$$

or

$$\Phi_i = A_i + B_i \cdot \exp\left(-\frac{\Delta G^0_{m,i}}{RT}\right) + \frac{C_i}{\exp\left(-\frac{\Delta G_{as,i}}{RT}\right) - \exp\left(-\frac{\Delta G^0_{m,i}}{RT}\right)}, \tag{9}$$

where $\Delta G_{as,I}$ is the Gibbs free energy of association, upon reaching which component (i) can be considered to have completely transformed into the associated state; A_i, B_i, C_i are empirical coefficients.

Equations (8) and (9) make it possible, from the standpoint of statistical thermodynamics, to explain the physical significance of the dependence of the osmotic coefficient Φ_i on the ratio of the activities of the crystallizing component under equilibrium conditions.

It should be noted that, depending on the nature of interparticle interactions in melts, different systems may exhibit different types of variation in Φ_i along the liquidus and solidus lines. As will be demonstrated below, if van der Waals forces of interaction between the elementary structural units of the component under consideration and the second component predominate in the melt along the liquidus line, a linear relationship is observed (where the term elementary structural units refers to atoms of elements or molecules of compounds).

When associates are formed from the initial components or when the compound under study undergoes dissociation in the melt, the actual number of atoms or molecules of the given phase will depend more strongly on the temperature and composition of the melt, according to highly complex relationships that include the degree of compound dissociation. This inevitably leads to a nonlinear dependence (6).

Expressions (5), (8), and (9) make it possible to derive semi-empirical relationships in the form of generalized Schröder–Le Chatelier equations for calculating the liquidus and solidus lines of any real system within the crystallization range of the corresponding phase according to the following relationships:

$$\begin{aligned} \frac{x_1^L}{x_1^S} &= \exp\left[\frac{\frac{\Delta H_{m,1}}{R}\left(\frac{1}{T_{m,1}} - \frac{1}{T}\right) + \int_T^{T_{m,1}}\left[\frac{1}{RT^2}\int_T^{T_{m,1}} \Delta C_{p,1} dT\right] dT}{\Phi_1'}\right] = M_r, \\ \frac{x_2^L}{x_2^S} &= \exp\left[\frac{\frac{\Delta H_{m,2}}{R}\left(\frac{1}{T_{m,2}} - \frac{1}{T}\right) + \int_T^{T_{m,2}}\left[\frac{1}{RT^2}\int_T^{T_{m,2}} \Delta C_{p,2} dT\right] dT}{\Phi_2'}\right] = N_r. \end{aligned} \tag{10}$$

The solution of the system of Equation (10) provides mathematical expressions for the solidus and liquidus lines of real systems:

$$x_{1,r}^{L} = M_r \cdot \frac{N_r - 1}{N_r - M_r}; \qquad x_{1,r}^{S} = \frac{N_r - 1}{N_r - M_r}. \tag{11}$$

These are the L and S equations for any type of phase diagram. In order for these equations to be applicable, it is first necessary to determine the empirical expressions (8) and (9) for each crystallizing phase.

In this paper, the second approach to the mathematical description of the phase equilibrium line (liquidus and solidus) is presented in the form of regular relationships for the Bjerrum–Guggenheim coefficients (Φ_i' and Φ_i'') (Equations (12) and (13)):

$$\Phi_i' = \left(\ln a_i^L / \ln a_i^S\right) / (\ln x_i^L / x_i^S) = (A_i + B_i) \cdot a_i^L / a_i^S, \tag{12}$$

$$\Phi_i'' = \left(\ln a_i^L / \ln a_i^S\right) / \ln x_i^L = (M_i + N_i) \cdot a_i^L / a_i^S. \tag{13}$$

These relationships, in turn, made it possible to derive semi-empirical expressions for calculating the liquidus and solidus lines of each crystallizing phase in the system under consideration:

$$\ln X_i^L = \frac{\Delta H_{m,i}}{R}\left(\frac{1}{T_{m,i}} - \frac{1}{T}\right) \cdot / \Phi_i'', \tag{14}$$

$$\ln X_i^S = \frac{\Delta H_{m,i}}{R}\left(\frac{1}{T_{m,i}} - \frac{1}{T}\right) \cdot \left(\frac{1}{\Phi_i''} - \frac{1}{\Phi_i'}\right), \tag{15}$$

where $\Delta H_{m,i}$—is the enthalpy of fusion of component *i* at its melting temperature, J/mol; R is the universal gas constant, 8.3144 J/(mol·K).

$T_{m,i}$ and T are the melting temperature of component *i* and the crystallization temperature of the melts, K;

Φ_i'—is the Bjerrum–Guggenheim coefficient for component *i*, used to establish a correlation dependence and obtain a mathematical expression for the ratio of the activities of component *i* in the liquid and solid phases;

Φ_i''—is the Bjerrum–Guggenheim coefficient for component *i*, used to establish a correlation dependence and obtain a mathematical expression for the liquidus line of component *i*.

For relationships (12) and (13), the equation coefficients were determined using the least squares method, with evaluation of the correlation coefficient $R_{x\gamma}$ (for linear dependence) or the convergence variance σ (for nonlinear dependence). All calculations were performed using software developed in the Delphi 7 programming environment.

3. Results

To gain insight into the behavior of magnesium in interaction with zinc within the multicomponent system Fe–Si–Al–Ca–Cu–Mg–Zn–Pb, an analysis of the Mg–Zn phase diagram was carried out in order to assess the degree of zinc sublimation through characteristic changes in the Bjerrum–Guggenheim osmotic coefficient.

With positive deviations of the numerical values of the osmotic coefficient from ideality ($\Phi_i > 1$), one may infer the predominance of interactions between like atoms. In contrast, when $\Phi_i < 1$, interactions between unlike atoms dominate in the melt, and the formation of complex high-temperature compounds becomes possible. Thus, the character of variation of the Bjerrum–Guggenheim osmotic coefficient relative to the activity ratio of components in ideal liquid and solid phases (positive $\Phi_i > 1$ or negative $\Phi_i < 1$) under the boundary

conditions of phase crystallization fields serves as direct evidence that, in the melt, zinc and lead are prone to forming volatile fractions [5].

3.1. Mathematical Description of Monovariant Phase Equilibrium Lines in the Form of the Semi-Empirical Schröder–Le Chatelier Dependence

The Mg–Zn phase diagram was described mathematically using a semi-empirical relationship based on the Schröder–Le Chatelier equation, which enables a unified analytical treatment of the liquidus and solidus lines for the crystallizing phases of the system.

3.1.1. Mg–Zn Phase Diagram

According to sources [7,8], the Mg–Zn system contains one congruently melting compound, $MgZn_2$, and three incongruently melting compounds: MgZn, Mg_2Zn_3, and Mg_2Zn_{11}. It is necessary to evaluate the degree of dissociation of the congruently melting compound $MgZn_2$ based on the behavior of the Bjerrum–Guggenheim osmotic coefficient.

To obtain numerical values of the Bjerrum–Guggenheim osmotic coefficient, composition and corresponding temperature data were taken from the phase diagram (Figure 1) for the two partial systems $MgZn_2$–Mg and $MgZn_2$–Zn. To calculate the activities of the liquid and solid phases for the ideal state of the system using Equation (1) of the Schröder–Le Chatelier equation, thermodynamic data were employed: $\Delta H_{m,MgZn2}$ = 48,621.17 J/mol and $T_{m,MgZn2}$ = 853 K [9,10].

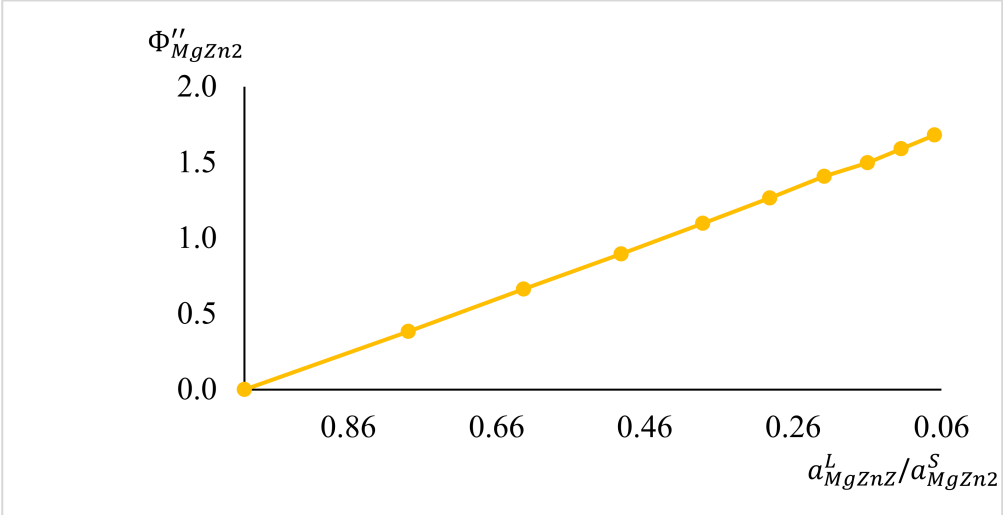


Figure 1. Graph of the Bjerrum–Guggenheim osmotic coefficient Φ''_{MgZn_2} versus the activity ratio of liquid and solid phases $a^L_{MgZn_2}/a^S_{MgZn_2}$ for the ideal state in the $MgZn_2$ crystallization region of the partial $MgZn_2$–Mg system.

The aim of this work is to determine how the $MgZn_2$ compound behaves in the melt—specifically, whether complex compounds, associates, or coordination-type structures are formed. Therefore, only the two quasi-crystallization regions $MgZn_2$–Mg and $MgZn_2$–Zn are of interest.

To recalculate the composition in terms of magnesium for the $MgZn_2$ crystallization region in the partial $MgZn_2$–Mg system, Equation (16) was used [11]:

$$x_1 = (Q_1 - (Q_1 + P_1)\cdot x_0)/((I_1 + J_1 - Q_1 - P_1)\cdot x_0 - I_1 + Q_1) \quad (16)$$

where x_1 is the concentration of the crystallizing compound in the melt relative to the partial system, i.e., the net concentration;

I_1, J_1, Q_1 and P_1 are the stoichiometric coefficients of the congruently melting compound $MgZn_2$ for the partial system $MgZn_2$–Mg within the Mg–Zn system. For this system: $I_1 = 1$, $J_1 = 2$, $Q_1 = 1$, $P_1 = 0$

Equation (16) was derived to recalculate the equilibrium compositions of the liquid and solid phases at a given temperature from the base system to the partial system, taking into account changes in the net concentrations of the melt components for the case of complete dissociation of the compound.

The initial data for the $MgZn_2$ crystallization region in the partial $MgZn_2$–Mg system are presented in Table 1.

Table 1. Initial data for the $MgZn_2$ crystallization region of the partial $MgZn_2$–Mg system.

T, K	x^L_{Mg}	x^S_{Mg}	$x^L_{MgZn_2\,recalc.}$	$lna^L_{MgZn_2}/a^S_{MgZn_2}$	$a^L_{MgZn_2}/a^S_{MgZn_2}$	Φ'_{MgZn_2}	Φ''_{MgZn_2}
853	0.333	0.333	1.000	0.000	1.000	0.000	0.000
823	0.490	0.333	0.520	−0.250	0.779	−0.648	0.383
798	0.505	0.333	0.490	−0.473	0.623	−1.137	0.663
773	0.525	0.333	0.452	−0.710	0.492	−1.562	0.894
748	0.546	0.333	0.416	−0.962	0.382	−1.950	1.097
723	0.570	0.333	0.377	−1.233	0.292	−2.297	1.264
698	0.596	0.333	0.339	−1.522	0.218	−2.619	1.407
673	0.630	0.333	0.294	−1.834	0.160	−2.880	1.496
648	0.662	0.333	0.255	−2.169	0.114	−3.161	1.588
614	0.710	0.333	0.204	−2.669	0.069	−3.529	1.680

3.1.2. $MgZn_2$–Mg Crystallization Region

Table 1 presents the initial composition and temperature data for the $MgZn_2$ crystallization region of the partial $MgZn_2$–Mg system. Also included are the numerical values of the Bjerrum–Guggenheim osmotic coefficient, calculated according to the methodology described above [2,11,12].

To recalculate the magnesium composition from the overall Mg–Zn system to the partial $MgZn_2$–Mg system using Equation (16), the obtained conversion coefficients were taken as I = 1, J = 2, Q = 1, and $p = 0$.

According to Table 1, the numerical values of the Bjerrum–Guggenheim osmotic coefficient were obtained and are graphically presented in Figure 1.

Using the least squares method (LSM), the equation describing the dependence of Φ''_{MgZn_2} on $a^L_{MgZn_2}/a^S_{MgZn_2}$ was obtained as follows (17):

$$\Phi''_{MgZn_2} = 1.7923 - 1.8045 \cdot a^L_{MgZn_2}/a^S_{MgZn_2}, \quad R_{xy} = -0.9999 \tag{17}$$

The expression for calculating the composition of the liquid phase within the temperature range 853 K–814 K is given by Equation (18):

$$\ln x^L_{MgZn_2-Mg} = \frac{\frac{48,621.17}{8.3143}\left(\frac{1}{853} - \frac{1}{T}\right) + \int_T^{T_{m,i}}\left[\frac{1}{RT^2}\int_T^{T_{m,i}} \Delta C_p dT\right] dT}{1.7923 - 1.8045 \cdot \exp\left[\frac{48,621.17}{8.3143}\left(\frac{1}{853} - \frac{1}{T}\right) + \int_T^{T_{m,i}}\left[\frac{1}{RT^2}\int_T^{T_{m,i}} \Delta C_p dT\right] dT\right]}. \tag{18}$$

Equations (17) and (18) made it possible to perform a comparative analysis of the calculated and experimental data, which is presented in Table 2.

Table 2. Comparative Analysis of Calculated and Experimental Data for the Magnesium Crystallization Region of the $MgZn_2$–Mg System.

T, K	Φ''_{MgZn_2}	$\Phi''_{MgZn_2,calc.}$	$lna^L_{MgZn_2}/a^S_{MgZn_2}$	$a^L_{MgZn_2}/a^S_{MgZn_2}$	$x^L_{MgZn_2}$	$x^L_{MgZn_2,calc.}$
853	0.000	−0.012	0.000	1.000	1.000	1.000
823	0.383	0.387	−0.250	0.779	0.520	0.524
798	0.663	0.667	−0.473	0.623	0.490	0.493
773	0.894	0.905	−0.710	0.492	0.452	0.456
748	1.097	1.103	−0.962	0.382	0.416	0.418
723	1.264	1.266	−1.233	0.292	0.377	0.378
698	1.407	1.399	−1.522	0.218	0.339	0.337
673	1.496	1.504	−1.834	0.160	0.294	0.295
648	1.588	1.586	−2.169	0.114	0.255	0.255
614	1.680	1.667	−2.669	0.069	0.204	0.202

3.1.3. $MgZn_2$–Zn Crystallization Region

For the $MgZn_2$ crystallization region of the partial $MgZn_2$–Zn system, the initial composition and temperature data are presented in Table 3. The compositions were recalculated from the base Mg–Zn system to the partial system using Equation (7).

Table 3. Initial data for the $MgZn_2$ crystallization region of the partial $MgZn_2$–Zn system.

T, K	x^L_{Mg}	x^S_{Mg}	$x^L_{MgZn2_{recacl.}}$	$lna^L_{MgZn_2}/a^S_{MgZn_2}$	$a^L_{MgZn_2}/a^S_{MgZn_2}$	Φ'_{MgZn_2}	Φ''_{MgZn_2}
853	0.333	0.333	1.000	0.000	1.000	0	0.000
823	0.210	0.333	0.362	−0.250	0.779	0.541	0.246
798	0.199	0.333	0.331	−0.473	0.623	0.916	0.427
773	0.184	0.333	0.291	−0.710	0.492	1.194	0.575
748	0.170	0.333	0.258	−0.962	0.382	1.429	0.709
723	0.153	0.333	0.220	−1.233	0.292	1.583	0.815
698	0.137	0.333	0.189	−1.522	0.218	1.712	0.913
673	0.118	0.333	0.154	−1.834	0.160	1.766	0.982
654	0.103	0.333	0.130	−2.086	0.124	1.776	1.021

Using the least squares method (LSM), the functional dependence of the Bjerrum–Guggenheim osmotic coefficient Φ''_{MgZn_2} on $a^L_{MgZn_2}/a^S_{MgZn_2}$ for the $MgZn_2$ crystallization region of the partial $MgZn_2$–Zn system (Figure 2) was determined and is expressed as Equation (19):

$$\Phi''_{MgZn2} = 1.1625 - 1.1730 \cdot a^L_{MgZn2g}/a^S_{MgZn2} \quad R_{xy} = -0.998 \tag{19}$$

The expression for calculating the composition within the temperature range 853 K–654 K is given by Equation (20):

$$\ln x^L_{MgZn_2-Zn} = \frac{\frac{48,621.17}{8.3143}\left(\frac{1}{853} - \frac{1}{T}\right) + \int_T^{T_{m,i}}\left[\frac{1}{RT^2}\int_T^{T_{m,i}} \Delta C_p dT\right]dT}{1.1625 - 1.1730 \cdot \exp\left[\frac{48,621.17}{8.3143}\left(\frac{1}{853} - \frac{1}{T}\right) + \int_T^{T_{m,i}}\left[\frac{1}{RT^2}\int_T^{T_{m,i}} \Delta C_p dT\right]dT\right]}. \tag{20}$$

A comparative analysis of the $MgZn_2$ composition calculated using Equations (19) and (20) is presented in Table 4.

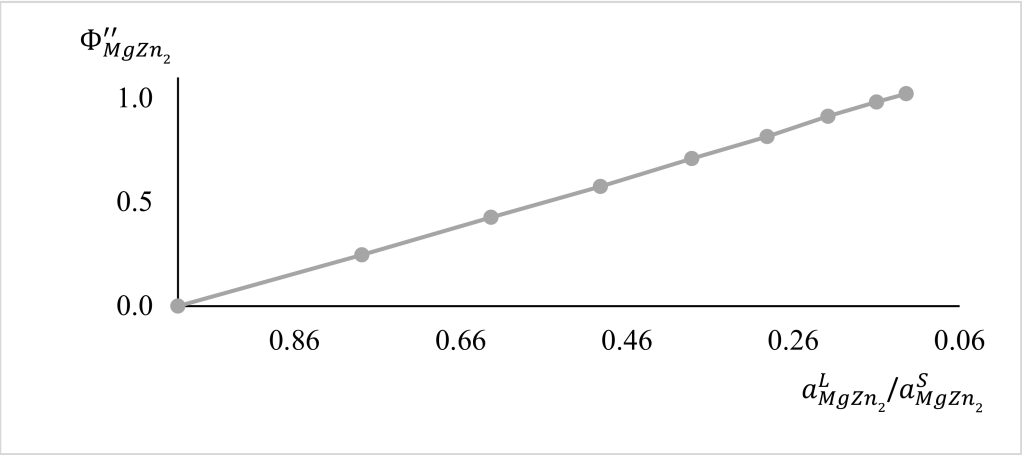


Figure 2. Graph of the Bjerrum–Guggenheim osmotic coefficient Φ''_{MgZn2} versus the activity ratio of liquid and solid phases $a^L_{MgZn_2}/a^S_{MgZn_2}$ for the ideal state in the $MgZn_2$ crystallization region of the partial $MgZn_2$–Zn system.

Table 4. Comparative analysis of calculated and experimental data for the $MgZn_2$ crystallization region of the $MgZn_2$–Zn system.

Φ''_{MgZn_2}	$\Phi''_{MgZn_2,calc.}$	$lna^L_{MgZn_2}/a^S_{MgZn2}$	$a^L_{MgZn_2}/a^S_{MgZn_2}$	$x^L_{MgZn_2}$	$x^L_{MgZn_2,calc.}$
0.000	−0.011	0.000	1.000	1.000	1.000
0.246	0.249	−0.250	0.779	0.362	0.366
0.427	0.432	−0.473	0.623	0.331	0.334
0.575	0.585	−0.710	0.492	0.291	0.297
0.709	0.714	−0.962	0.382	0.258	0.260
0.815	0.820	−1.233	0.292	0.220	0.222
0.913	0.907	−1.522	0.218	0.189	0.187
0.982	0.975	−1.834	0.160	0.154	0.152
1.021	1.017	−2.086	0.124	0.130	0.129

Figure 3 shows a schematic representation of the crystallization region of the congruently melting compound $MgZn_2$, with the calculated composition plotted according to Equation (9) for the Mg–$MgZn_2$ region and Equation (11) for the $MgZn_2$–Zn region. The phase diagram of this system is a simple eutectic type, with no solid-state solubility and with the formation of a congruent compound. The calculated compositions obtained in the present study are in good agreement with the liquidus curve and phase compositions reported by William Hume-Rothery and Geoffrey V. Raynor [7,8].

The analysis of the behavior of the Bjerrum–Guggenheim osmotic coefficient in the Mg–Zn system for the two partial systems $MgZn_2$–Mg and $MgZn_2$–Zn showed that only van der Waals interactions occur between the components in the melt. The graphs of Φ''_{MgZn_2} versus $a^L_{MgZn_2}/a^S_{MgZn_2}$ exhibit a strictly correlational dependence.

The Mg–Zn system contains three incongruently melting compounds: MgZn, Mg_2Zn_3 и Mg_2Zn_{11}. However, the correlation analysis of the Bjerrum–Guggenheim coefficient indicates that no associates are formed in the melt, and the degree of dissociation of $MgZn_2$ is very high, even when judged by the dome shape of the liquidus line of the congruent compound.

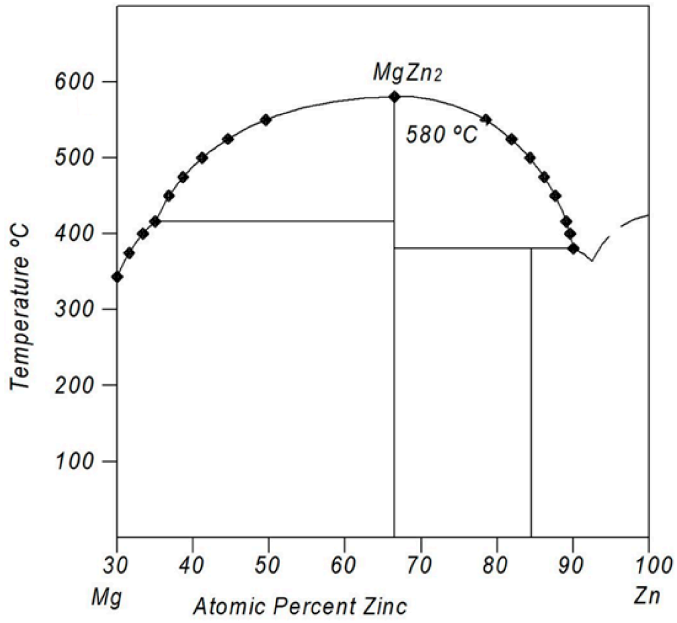


Figure 3. Schematic representation of the crystallization region of the congruently melting $MgZn_2$ compound with the calculated compositions in the Mg–$MgZn_2$ and $MgZn_2$–Zn regions.

3.2. Assessment of the Degree of Dissociation of the Congruent Compound $MgZn_2$

The theoretical analysis of the behavior of the Bjerrum–Guggenheim osmotic coefficient graphs near the melting temperatures of chemical compounds made it possible to apply an equilibrium method for calculating the dissociation parameters of a congruent compound based on the analysis of the monovariant equilibrium line [11,13].

The demonstrated method of mathematically describing monovariant phase equilibrium lines through the Bjerrum–Guggenheim osmotic coefficient allowed the direct Gibbs problem to be solved and provided an accurate mathematical representation of the $MgZn_2$ crystallization fields for the partial systems in the form of modified Schröder–Le Chatelier Equations (9) and (11), describing the actual positions of the liquidus and solidus lines on the phase diagram.

Using the developed software for calculating the Gibbs energy of hetero-homogeneous reactions (based on the method of M.I. Temkin and L.A. Shvartsman [14]), the equilibrium constant (K_r) and the degree of dissociation (α) of $MgZn_2$ were calculated via the Bjerrum–Guggenheim osmotic coefficient for the $MgZn_2$ dissociation reaction. Gibbs energies for the dissociation reaction of $MgZn_2$, equilibrium constants along the monovariant phase equilibrium lines, and the degree of dissociation of $MgZn_2$ were determined for the quasi-systems $MgZn_2$–Mg and $MgZn_2$–Zn.

The calculated data are presented in Tables 5 and 6.

The correctness of the performed calculations is confirmed by the linearity of the graphs showing the dependence of Φ''_{MgZn2} on $a^L_{MgZn2,}/a^S_{MgZn2}$ taking into account the degree of dissociation (Figures 2 and 3). Indirectly, through the Bjerrum–Guggenheim osmotic coefficient, the degree of dissociation of $MgZn_2$ in the Mg–Zn system was determined to range from 17% to 46%, which is also in good agreement with the conclusions of Nikolay Semyonovich Kurnakov [15] regarding the smooth maximum for $MgZn_2$—that is, the composition of the liquid phase changes continuously with deviation from stoichiometry, resulting in a symmetrical rounded peak.

Table 5. Calculated thermodynamic data for the $MgZn_2$ crystallization region in the $MgZn_2$–Mg system.

T, K	ΔGr J/mol	ΔHr J/mol	ΔSr J/mol·K	Kr	Degree of Dissociation α
853	−2323.91	5631.92	9.33	1.39	0.76
823	−2024.35	6731.61	10.64	1.34	0.35
798	−1744.94	7599.70	11.71	1.31	0.32
773	−1439.56	8424.54	12.76	1.25	0.28
748	−1107.16	9204.83	13.79	1.19	0.24
723	−749.92	9942.22	14.79	1.13	0.21
698	−367.94	10,636.41	15.77	1.07	0.17
673	−180.04	3277.94	5.14	1.03	0.16
648	−57.77	2951.56	4.64	1.01	0.09
614	88.81	2532.78	3.98	0.98	0.05

Table 6. Calculated thermodynamic data for the $MgZn_2$ crystallization region in the $MgZn_2$–Zn system.

T, K	ΔGr J/mol	ΔHr J/mol	ΔSr J/mol · K	Kr	Degree of Dissociation α
853	−2323.91	5631.92	9.33	1.39	0.76
823	−2024.35	6731.61	10.64	1.34	0.21
798	−1744.94	7599.70	11.71	1.30	0.18
773	−1439.02	8424.05	12.76	1.25	0.14
748	−1107.16	9204.83	13.79	1.20	0.11
723	−749.92	9942.22	14.79	1.13	0.07
698	−367.94	10,636.41	15.77	1.06	0.04
673	−180.04	3277.94	5.14	1.03	0.02
654	−85.99	3028.46	4.76	1.01	0.01

3.3. Experimental Section

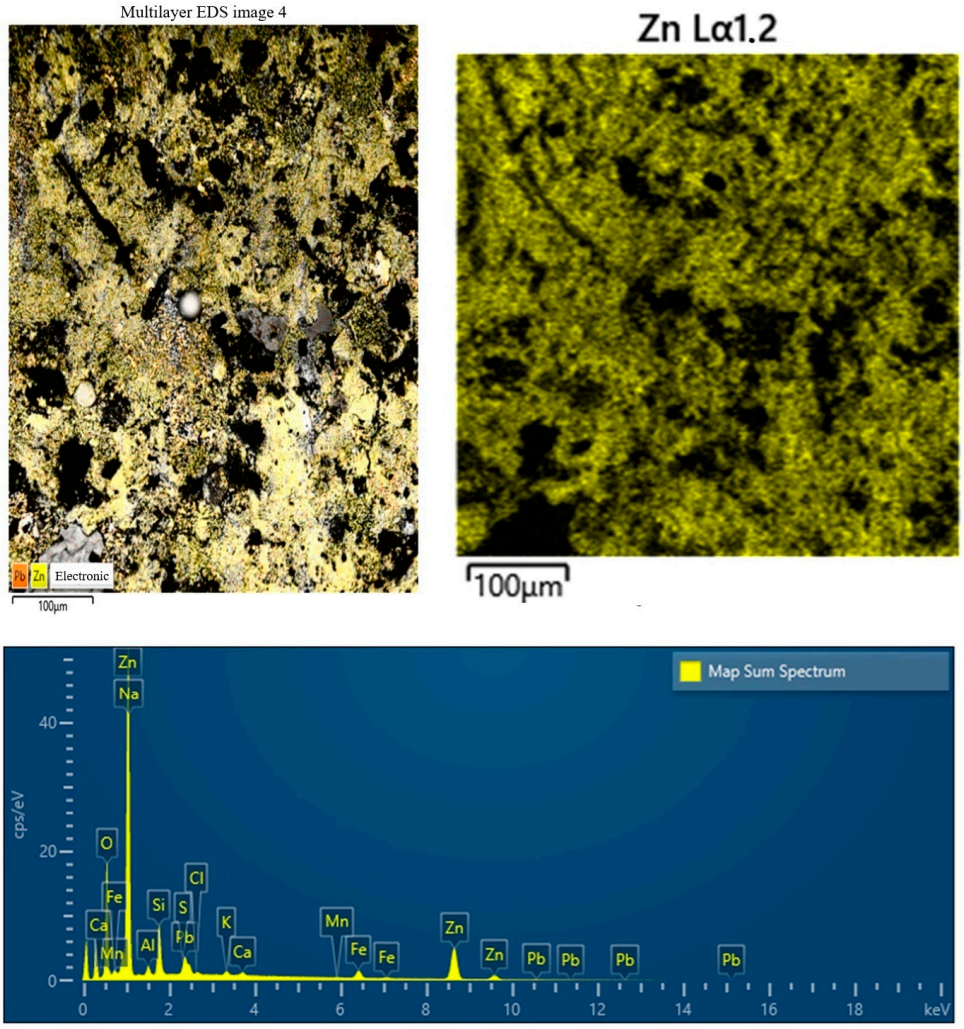
To validate the theoretical analysis of zinc sublimation based on the Bjerrum–Guggenheim concept, an experimental study of copper smelting slag was carried out.

The aim of the experimental part was to verify the theoretical conclusions on zinc behavior, in particular to confirm its sublimation and to study the morphology and distribution of zinc-containing phases in the metal smelting products obtained from multicomponent slag in an electric arc furnace [16–18].

Scanning electron microscopy (SEM) with energy-dispersive X-ray spectroscopy (EDS) was used for the analysis. Three types of samples were studied: the original slag, the metallic phase obtained after smelting, and dust collected in the flue ducts.

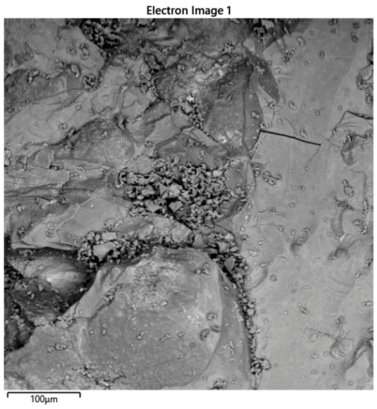
SEM analysis revealed the following:

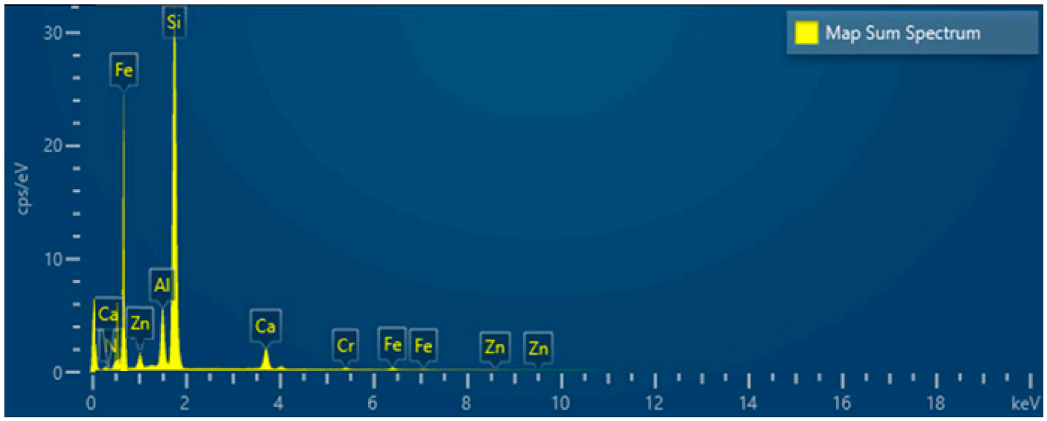
1. The initial component composition of the slag is shown in Figure 4. As is known, in the slag phase, zinc is present in the form of oxide compounds.
2. In the metallic phase presented in Figure 5, morphological analysis showed that zinc is present as fine dispersed inclusions.
3. More localized elemental analysis (EDS) in different zones of dust particles showed the presence of zinc-enriched particles, confirming the process of significant zinc sublimation followed by condensation. Two analyses of representative samples are presented in Figures 6 and 7.



Map Sum Spectrum							
Element	Line Type	Weight %	Weight % Sigma	Atomic %	Oxide	Oxide %	Oxide % Sigma
O	K series	24.44	0.11	52.19			
Na	K series	4.86	0.16	7.22	Na_2O	6.55	0.22
Al	K series	1.13	0.03	1.43	Al_2O_3	2.13	0.06
Si	K series	5.46	0.04	6.64	SiO_2	11.67	0.09
S	K series	0.50	0.03	0.54	SO_3	1.26	0.08
Cl	K series	0.18	0.02	0.17		0.00	0.02
K	K series	0.60	0.03	0.53	K_2O	0.72	0.03
Ca	K series	0.49	0.03	0.42	CaO	0.69	0.04
Mn	K series	0.18	0.05	0.11	MnO	0.24	0.07
Fe	K series	4.43	0.08	2.71	FeO	5.7	0.10
Zn	L series	51.79	0.17	27.07	ZnO	64.46	0.21
Pb	M series	5.94	0.13	0.98	PbO	6.4	0.14
Total		100.00		100.00		99.82	

Figure 4. SEM Images of the slag phase and the corresponding overall elemental map spectrum of the initial slag phase, showing the presence of zinc as oxide compounds.





Map Sum Spectrum				
Element	Line Type	Weight %	Weight % Sigma	Atomic %
Si	K series	50.00	0.16	63.04
Al	K series	9.09	0.07	11.90
Cr	K series	1.73	0.13	1.18
Fe	K series	36.42	0.21	22.79
Zn	L series	2.74	0.18	1.09
Total		100.00		100.00

Figure 5. SEM Image of Inclusions in the Metal and the Corresponding Overall Elemental Spectrum of the Metallic Phase.

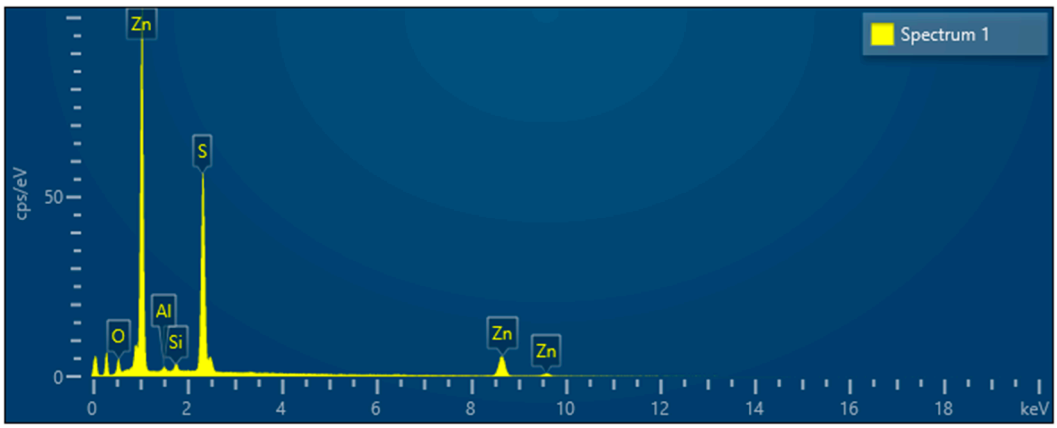
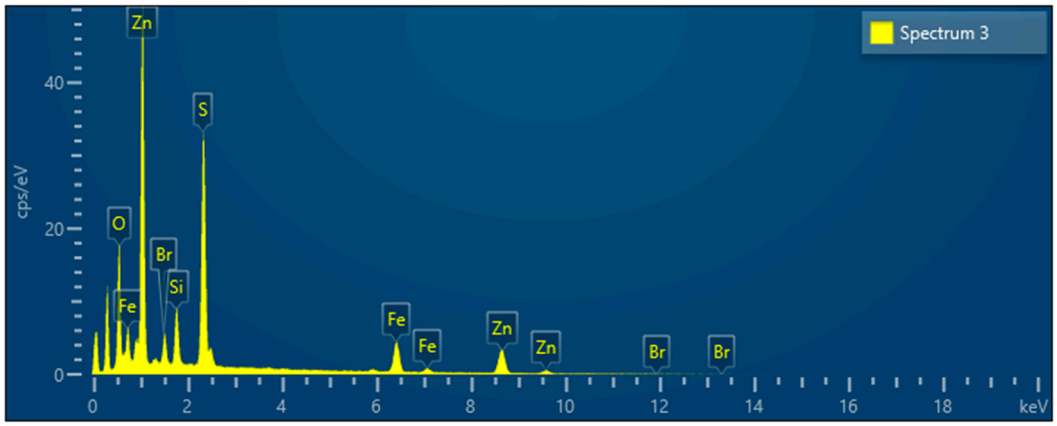


Figure 6. *Cont.*

Map Sum Spectrum				
Element	Line Type	Weight %	Weight % Sigma	Atomic %
O	K series	5.61	0.16	13.76
Mg	K series	1.77	0.06	2.86
Al	K series	3.47	0.06	5.05
Si	K series	12.06	0.08	16.86
S	K series	24.33	0.10	29.79
Zn	L series	52.76	0.16	31.68
Total		100.00		100.00

Figure 6. Overall elemental spectrum results of the dust phase, analysis 1.



Spectrum 3				
Element	Line Type	Weight %	Weight % Sigma	Atomic %
O	K series	17.15	0.21	39.42
Si	K series	4.06	0.08	5.32
S	K series	17.55	0.15	20.12
Fe	K series	12.32	0.21	8.12
Zn	L series	44.09	0.26	24.80
Br	L series	4.83	0.16	2.22
Total		100.00		100.00

Figure 7. Overall elemental spectrum results of the dust phase, analysis 2.

4. Discussion

The present study demonstrates that the Bjerrum–Guggenheim osmotic coefficient can serve as an informative thermodynamic parameter for analyzing the structural state of liquid metallic systems and evaluating the stability of congruently melting compounds. In the Mg–Zn system, the obtained dependencies made it possible not only to mathematically describe the monovariant phase equilibrium lines with high accuracy but also to assess the degree of dissociation of the $MgZn_2$ compound and to explain the mechanism of zinc volatilization during high-temperature processing [19,20].

The linear relationships obtained between the Bjerrum–Guggenheim osmotic coefficient and the activity ratio of the liquid and solid phases for both partial systems, $MgZn_2$–Mg and $MgZn_2$–Zn, are of particular importance. The correlation coefficients approaching

unity indicate that the proposed modification of the Schröder–Le Chatelier equation adequately reproduces the real behavior of the crystallization boundaries. Such agreement suggests that the osmotic coefficient can be regarded as a sensitive indicator of changes occurring in the melt structure near phase equilibrium conditions. The observed regularity also confirms the applicability of the proposed methodology for describing phase equilibria in systems containing congruently melting compounds [21].

The obtained values of the Bjerrum–Guggenheim coefficient provide insight into the nature of interparticle interactions in the liquid alloy. The analysis showed that the Mg–Zn melt is characterized predominantly by weak interactions, which may be interpreted as the absence of stable associates or long-lived structural units in the liquid phase. This conclusion is noteworthy because the phase diagram contains several intermetallic compounds, namely MgZn, $MgZn_2$, and $MgZn_5$ [22]. Nevertheless, the behavior of the osmotic coefficient indicates that these compounds do not preserve their structural identity in the melt and are largely dissociated into simpler atomic species. Such behavior is consistent with the concept that the structure of the liquid alloy is governed mainly by short-range interactions rather than by the existence of persistent complex clusters.

A key result of the present work is the determination of the degree of dissociation of $MgZn_2$. The calculated values ranging from approximately 17% to 46% indicate that the compound possesses only moderate thermodynamic stability under the investigated conditions. Consequently, a considerable fraction of $MgZn_2$ is dissociated in the melt, generating free magnesium and zinc species. The progressive increase in the degree of dissociation along the phase equilibrium line suggests that the compound cannot be considered a completely stable structural entity in the liquid state. This finding is important because the concentration of free zinc atoms directly influences zinc activity and, therefore, its tendency to volatilize during metallurgical processing.

The calculated dissociation behavior is in good agreement with the classical concepts developed by Kurnakov concerning the relationship between the shape of phase diagram maxima and the stability of congruent compounds. According to this approach, a sharp and narrow liquidus maximum corresponds to a highly stable compound with limited dissociation, whereas a broad and smooth maximum indicates significant dissociation in the melt. The liquidus dome of $MgZn_2$ is characterized by a relatively rounded and symmetrical shape, which is consistent with the calculated dissociation degree. Therefore, the thermodynamic interpretation derived from the Bjerrum–Guggenheim coefficient independently confirms the conclusions that can be drawn from the geometric characteristics of the phase diagram. The agreement between these two approaches supports the physical validity of the proposed methodology.

The thermodynamic calculations further suggest that the $MgZn_2$ compound exists in a dynamic equilibrium between associated and dissociated states. The values of Gibbs free energy, equilibrium constants, and dissociation degree indicate that the system remains close to equilibrium throughout the investigated temperature interval. Under such conditions, even moderate changes in temperature or chemical environment may alter the concentration of free zinc in the melt. This behavior is particularly important for metallurgical systems containing volatile components because the activity of zinc is one of the primary factors controlling its transfer into the gas phase [23,24].

The obtained samples were investigated using a scanning electron microscope (SEM) Zeptools ZEM20 (ZEPTOOLS, Tongling, China) equipped with an Oxford energy-dispersive spectroscopy (EDS) detector (Oxford Instruments, Abingdon, UK). The experimental SEM/EDS results provide independent confirmation of the thermodynamic predictions. The initial slag contains zinc predominantly in oxide form, with concentrations exceeding 50 wt.%, demonstrating that zinc is one of the major components of the investigated mate-

rial. After carbothermic treatment, zinc was detected only in relatively small quantities in the metallic phase and mainly as finely dispersed inclusions. Such morphology suggests that a substantial portion of zinc does not remain dissolved in the metal but is instead removed from the reaction zone. The most convincing evidence of this process is the presence of zinc-rich particles in the collected dust, where local zinc concentrations reached approximately 44 wt.%. The occurrence of such particles strongly supports the assumption that zinc undergoes evaporation followed by condensation in cooler sections of the gas path [25].

The consistency between the theoretical and experimental results deserves special attention. The thermodynamic analysis predicts a relatively high degree of dissociation of $MgZn_2$ and weak interactions within the melt structure, both of which favor the formation of free zinc species. Experimental observations, in turn, reveal significant zinc enrichment in the dust phase and reduced zinc content in the metallic product. These findings indicate that volatilization is the dominant mechanism governing zinc redistribution during processing [26]. Thus, the SEM/EDS investigation serves not merely as an auxiliary characterization technique but as direct evidence supporting the thermodynamic interpretation derived from phase diagram analysis.

From a practical perspective, the obtained results are relevant for the processing of zinc-containing slags and other polymetallic technogenic materials. The demonstrated tendency of zinc to volatilize may be used advantageously in processes aimed at selective zinc recovery through controlled sublimation and subsequent condensation. At the same time, uncontrolled zinc evaporation may lead to metal losses and increased dust generation. Therefore, understanding the relationship between melt structure, compound dissociation, and zinc activity is essential for optimizing process parameters and improving metal recovery efficiency [27].

Despite the encouraging results, several limitations should be noted. The present analysis was performed using a binary Mg–Zn model system, whereas industrial slags represent considerably more complex multicomponent systems containing iron, silicon, calcium, aluminum, lead, copper, and other elements. These components may influence zinc activity through additional interactions not accounted for in the current thermodynamic treatment [28,29]. Furthermore, the degree of dissociation was evaluated indirectly through the behavior of the Bjerrum–Guggenheim coefficient and phase equilibrium data. Additional experimental investigations employing high-temperature structural characterization techniques could provide further verification of the proposed interpretation of melt structure.

Overall, the results demonstrate that the Bjerrum–Guggenheim osmotic coefficient represents a useful tool for investigating the thermodynamic behavior of metallic melts and assessing the stability of congruent compounds. The combination of phase diagram analysis, thermodynamic modeling, and experimental SEM/EDS characterization provides a consistent explanation for the high volatility of zinc in the Mg–Zn system and establishes a theoretical basis for predicting the behavior of volatile components during the pyrometallurgical processing of complex raw materials.

5. Conclusions

Theoretical studies were conducted on the behavior of the Bjerrum–Guggenheim osmotic coefficient (positive $\Phi_i < 1$ or negative $\Phi_i > 1$) in melts of the magnesium binary system Mg–Zn. This system is characterized by the formation of the congruent compound $MgZn_2$. Theoretical analysis showed that, when recalculated for partial systems, the graphs of the Bjerrum–Guggenheim osmotic coefficient exhibit a strictly correlational dependence, indicating that only van der Waals interactions—the weakest interactions in the melt—

are present. Applying Kurnakov's method on the curvature of the liquidus line of the congruent compound, it can be concluded that the liquidus dome of $MgZn_2$ is very smooth, which implies a high degree of dissociation and no obstacles to its significant sublimation.

(1) The estimation of the degree of dissociation (association) of the congruently melting compound $MgZn_2$ through the Bjerrum–Guggenheim osmotic coefficient, using the Gibbs energy of the dissociation reaction and the reaction equilibrium constant, makes it possible to determine the extent to which congruently melting compounds dissociate during melting.
(2) It was established that the degree of dissociation of the $MgZn_2$ compound at the moment of melting reaches 79%.
(3) Experimental data confirm the theoretically predicted substantial zinc sublimation under carbothermic processing conditions. The detection of zinc in the collected dust demonstrates its volatility, while its presence in the slag predominantly in oxide form (ZnO) indicates potential mechanisms of zinc loss. The theoretically predicted zinc volatility, based on the Bjerrum–Guggenheim concept, was validated experimentally.
(4) The form of zinc distribution in various phases was established: in the initial slag, zinc is primarily present as oxide compounds (ZnO), confirmed by elemental analysis, with a content of up to 51.79 wt.%. In the metallic phase after smelting, zinc occurs as fine dispersed inclusions, indicating partial reduction and distribution within the metal. In the collected dust (flue ducts), particles enriched with zinc (up to 44.09 wt.% by local EDS analysis) were identified, providing direct evidence of sublimation followed by condensation from the gas phase.
(5) Morphological analysis and the distribution of zinc-containing phases indicate that the main mechanism of zinc loss is volatilization and entrainment with the gas stream in the form of volatile compounds, with residual zinc remaining in the metal as dispersed inclusions.
(6) The use of SEM/EDS allowed for effective visualization and quantitative assessment of zinc distribution across all investigated processing products (slag, metal, and dust), confirming the adequacy of the chosen methodology for the objectives of this study. Thus, the experimental data unequivocally confirm the high volatility of zinc in the studied process and identify the key zinc-concentrating phases, which is consistent with theoretical predictions and explains the mechanism of zinc behavior during high-temperature processing of zinc-containing slags.

Author Contributions: Conceptualization, S.B.; Methodology, V.T.; Formal analysis, V.T., Y.M. and A.O.; Investigation, A.A. and A.O.; Data curation, A.A. and O.K.; Validation, V.T., A.A. and Y.M.; Writing—original draft preparation, V.T.; Writing—review and editing, S.B., Y.M., A.O. and O.K.; Supervision, S.B.; Project administration, V.T. All authors have read and agreed to the published version of the manuscript.

Funding: This research is funded by the Science Committee of the Ministry of Science and Higher Education of the Republic of Kazakhstan (Grant No. AP26194293).

Data Availability Statement: The original contributions presented in this study are included in the article. Further inquiries can be directed to the corresponding author.

Acknowledgments: All experimental samples, including magnesium–zinc alloys, slags, metallic products, and dust materials analyzed in this study, were obtained from industrial processing operations with appropriate authorization for research purposes. Analytical investigations were carried out using certified laboratory equipment in accordance with established experimental procedures.

Conflicts of Interest: The authors declare no conflicts of interest.

References

1. Podusovskaya, N.V.; Komolova, O.A.; Grigorovich, K.V.; Demin, K.Y.; Anisonyan, K.G. Analysis of Lead and Zinc Selective Extraction Process from EAF Dust during Carbothermic Reduction. *Russ. Metall.* **2025**, *3*, 14–31. [CrossRef]
2. Wang, D.; Yang, S.; Liu, X.; Duh, J.G.; Wang, C. Experimental Investigation and Thermodynamic Calculation of Phase Equilibria in the Mg–Pb–Zn Ternary System. *Mater. Chem. Phys.* **2016**, *171*, 227–238. [CrossRef]
3. Gu, M.; Zhong, Y.; Wang, L.; Guo, Z. Separation of Heavy Metals from Hazardous Lead Slag by Carbothermic Reduction and Thermal Volatilization: Effect of Phase Transformation on Sn, Pb, Zn Removal. *Process. Saf. Environ. Prot.* **2021**, *156*, 330–339. [CrossRef]
4. Tolokonnikova, V.; Baisanov, S.; Yerekeyeva, G.; Narikbayeva, G.; Korsukova, I. Evaluation of the Degree of Dissociation of a Congruent Compound Fe_2Ti across the Bjerrum–Guggenheim Coefficient. *Metals* **2022**, *12*, 2132. [CrossRef]
5. Tolokonnikova, V.V.; Baisanov, S.O.; Saulebek, Z.K.; Orlov, A.S. Mathematical Description of the Lines of Monovariant Phase Equilibria on the MnO–SiO_2 Phase Equilibrium Diagram. *CIS Iron Steel Rev.* **2023**, *26*, 105–110. [CrossRef]
6. Glazov, V.M.; Pavlova, L.M. *Chemical Thermodynamics and Phase Equilibria*; Metallurgy: Moscow, Russia, 1988; 555p.
7. Hume-Rothery, V.; Raynor, G. *Structure of Metals and Their Alloys*; Metallurgizdat: Moscow, Russia, 1958; 391p.
8. Bannykh, O.A.; Budberg, P.B.; Alisova, S.P.; Guzey, L.S.; Drits, M.E.; Dobatkina, T.V.; Lysova, E.V.; Nikitina, N.I.; Padezhnova, E.M.; Rokhlin, L.L.; et al. *Phase Diagrams of Binary and Multicomponent Iron-Based Systems*; Metallurgy: Moscow, Russia, 1986.
9. Glushko, V.P. *Thermodynamic Properties of Individual Substances (Handbook)*; VINITI Institute of High Temperatures of the USSR Academy of Sciences: Moscow, Russia, 1982; Volume 4, 456p.
10. Scientific Group Thermodata Europe. FACTSAGE Thermodynamic Database and Software, 2017. Available online: https://www.factsage.com/ (accessed on 10 March 2023).
11. Tolokonnikova, V. *Study of Thermal Stability of Congruently Melting Compounds for Model Systems Based on the Concept of the Bjerrum–Guggenheim Osmotic Coefficient*; Sanat-Poligrafiya: Karaganda, Kazakhstan, 2022; 117p.
12. Akberdin, A.A.; Kim, A.S.; Sultangaziev, R.B.; Orlov, A.S. The Method of Mathematical Description of the Phase Composition Diagrams. *CIS Iron Steel Rev.* **2023**, *25*, 79–83. [CrossRef]
13. Tolokonnikova, V.; Baisanov, S.; Narikbayeva, G.; Narikbayeva, I. Assessment of Dissociation Rate of $FeCr_2O_4$ Using the Bjerrum–Guggenheim Coefficient. *Metalurgija* **2021**, *60*, 303–305.
14. Ruzinov, L.P.; Gulyanitsky, V.S. *Equilibrium Transformations of Metallurgical Reactions*; Metallurgy: Moscow, Russia, 1975; 417p.
15. Kurnakov, N.S. *Selected Works*; Publishing House of the Academy of Sciences of the USSR: Moscow, Russia, 1961; Volume 1, 635p.
16. Horiuchi, T.; Ono, A.; Yoshioka, K.; Watanabe, T.; Ohkubo, K.; Mohri, T. Liquid–Solid Equilibrium and Intermediate Phase Formation during Solidification in Mg–1.3 at.% Zn–1.7 at.% Y Alloy. *Mater. Trans.* **2008**, *49*, 2247–2253.
17. Erofeev, K.B. Computer Modeling of Thermodynamic Properties of Liquid Binary Magnesium Alloys with Elements of Groups II–V of the Periodic Table. Ph.D. Thesis, St. Petersburg State Polytechnic University, St. Petersburg, Russia, 2005; 27p.
18. Bobryshev, B.L.; Moiseev, V.S.; Aleksandrova, Y.P.; Moiseev, K.V.; Bobryshev, D.B.; Bondarev, A.B. Improvement of Complex Processing of Magnesium Alloys during Melting. *Tekhnologiya Legk. Splav.* **2021**, *3*, 35–44.
19. Pelton, A.D. *Phase Diagrams and Thermodynamic Modeling of Solutions*; Elsevier: Amsterdam, The Netherlands, 2019.
20. Kerry, T.; Peters, A.; Georgakopoulos, E.; Dugulan, I.; Meijer, K.; Hage, J.; Offerman, E.; Yang, Y. Zinc Vaporization and Self-Reduction Behavior of Industrial Waste Residues for Recycling to the HIsarna Furnace. *J. Sustain. Metall.* **2022**, *8*, 658–672. [CrossRef]
21. Liang, P.; Seifert, H.J.; Lukas, H.L.; Ghosh, G.; Effenberg, G.; Aldinger, F. Thermodynamic Modelling of the Cu–Mg–Zn Ternary System. *Calphad* **1998**, *22*, 527–544. [CrossRef]
22. Leuchtenmueller, M.; Legerer, C.; Brandner, U.; Antrekowitsch, J. Carbothermic Reduction of Zinc-Containing Industrial Wastes: A Kinetic Model. *Metall. Mater. Trans. B* **2021**, *52*, 548–557. [CrossRef]
23. Ghosh, G.; Olson, G.B. Critical Assessment and Thermodynamic Modeling of the Mg–Zn, Mg–Sn, Sn–Zn and Mg–Sn–Zn Systems. *Calphad* **2012**, *36*, 28–43. [CrossRef]
24. Pauerová, K.; Dzurňák, R.; Trpčevská, J.; Liptai, P.; Vindt, T. An Experimental Study of Zinc Evaporation from Bottom Zinc Dross at Atmospheric Pressure and in Inert Atmosphere with Integrated CFD Modelling. *Materials* **2024**, *17*, 4627. [CrossRef] [PubMed]
25. Ma, S.; Zhang, Z.; Xu, S.; Li, X.; Feng, L. Recovery of Zinc from Electric Arc Furnace Dust by Vacuum Carbothermal Reduction. *Metall. Res. Technol.* **2021**, *118*, 415. [CrossRef]
26. Jha, M.K.; Kumar, V.; Singh, R.J. Review of Hydrometallurgical Recovery of Zinc from Industrial Wastes. *Resour. Conserv. Recycl.* **2001**, *33*, 1–22. [CrossRef]
27. Nowińska, K.; Adamczyk, Z. Zinc and Lead Metallurgical Slags as a Potential Source of Metal Recovery: A Review. *Materials* **2023**, *16*, 7295. [CrossRef] [PubMed]

28. Jeon, J.; Lindberg, D. Thermodynamic Optimization and Phase Equilibria Study of the MgO–ZnO, CaO–ZnO, and CaO–MgO–ZnO Systems. *Ceram. Int.* **2023**, *49*, 12736–12744. [CrossRef]
29. Jak, E.; Hayes, P.C.; Pelton, A.D.; Decterov, S. Thermodynamic Modelling of the Al_2O_3–CaO–FeO–Fe_2O_3–PbO–SiO_2–ZnO System with Addition of K and Na with Metallurgical Applications. In Proceedings of the VIII International Conference on Molten Slags, Fluxes and Salts (Molten 2009), Santiago, Chile, 18–21 January 2009; pp. 473–490.

Disclaimer/Publisher's Note: The statements, opinions and data contained in all publications are solely those of the individual author(s) and contributor(s) and not of MDPI and/or the editor(s). MDPI and/or the editor(s) disclaim responsibility for any injury to people or property resulting from any ideas, methods, instructions or products referred to in the content.